Optics and Lasers in Engineering 161 (2023) 107350

Contents lists available at ScienceDirect

Optics and Lasers in Engineering

journal homepage: www.elsevier.com/locate/optlaseng

Wavefront optical spacing of freeform surfaces and its measurement using CGH interferometry

Xin Zhang[a,b], Haixiang Hu[a,b,*], Donglin Xue[a,b,*], Qiang Cheng[a,b], Xi Yang[a,b], Wa Tang[a], Guanbo Qiao[a,b], Xuejun Zhang[a,b]

[a] Changchun Institute of Optics, Fine Mechanics and Physics, Chinese Academy of Sciences, Changchun, Jilin 130033, China
[b] University of Chinese Academy of Sciences, Beijing 100049, China

ARTICLE INFO

Keywords:
Freeform surface
Interferometric compensating test
Wavefront optical spacing
Cat-eye computer-generated hologram

ABSTRACT

For optical surfaces, the distance between the wavefront at ideal design position and that at real surface testing position along the wavefront propagation direction is an important parameter. It determines the on-axis curvature deviation and best-fit sphere radius of the surface under testing, and thus, affects the optical distance, effective focal length, and tolerance design of the optical system. We define the distance as wavefront optical spacing (WOS or spacing *d*). The analytical form of the WOS can be utilised in critical tolerance balancing, and its test results can aid in optical system redesign. Aiming at a computer-generated hologram (CGH) interferometric test, in this study, we propose the WOS concept and deduce the coupling relation between the surface error and spacing *d*, particularly in freeform surface conditions. A cat-eye CGH interferometric method was presented to test the spacing error within a precision of several microns. The simulation and error budget demonstrate that this method can measure the WOS of freeform surfaces. The experimental results indicate that the metrology accuracy is 10.2 ± 4.3 μm (P = 95%) (absolute accuracy), 4.5 μm (repeatability), and 2.1 ppm (relative accuracy).

1. Introduction

In the design of optical systems, freeform surfaces are widely used in military, aerospace, automobile, and illumination applications to meet the requirements of correcting aberrations, effectively simplifying structures, and improving image quality [1–5]. The final performance of an optical system depends on several factors. In addition to the optical design, the quality of the surface, geometric parameters, and adjustment position play a significant role [6,7]. Simply viewed, the most important factors for high-precision optical systems are surface figure quality and geometric parameters [8]. The interferometric compensation test, one of the most effective means of testing nano-accuracy freeform surfaces, is widely employed in optical surface figure testing [9,10]. Under the condition of the interferometric compensation test, six degrees of freedom exist for testing the geometric parameters. Among them, two translational degrees of freedom, perpendicular to the optical axis, and three rotational degrees of freedom are strictly limited by the designed interferometric compensator, which are adjustment quantities. The remaining degrees of freedom along the wavefront propagation direction are limited by the optics, which is an eigenvalue. In the interferometric compensating test, owing to geometric parameter error, the real surface has a distance along the direction of wavefront propagation with the ideal design surface, making the real surface mismatch the ideal design wavefront. We define the distance between the wavefront at the ideal design position and that at real surface testing position along the wavefront propagation direction as wavefront optical spacing (WOS or spacing *d*), as shown in Fig. 1. The WOS determines the focal length of the optical element and affects the tolerance design and system adjustment of an optical system. The analytical form of the WOS can be used for critical tolerance balancing, and its test results can be helpful in optical system redesign. In addition, the WOS has different forms for different surfaces. As shown in Fig. 1(a), spacing *d* is defined as the radius of curvature error in the test process for spherical surfaces. Additionally, for aspheric surfaces, as shown in Fig. 1(b), spacing *d* affects the vertex radius of the curvature and conic constant. For freeform surfaces, the relationship between the spacing *d* and the wavefront becomes complex, as shown in Fig. 1(c). The existence of WOS introduces extra surface testing error, affects the surface test results, and has an impact on the imaging quality of the optical system.

Accurate measurement of WOS is important for high-precision optical systems. Some techniques to test the radius of curvature or vertex radius of curvature and conic constant under the conditions of the interferometric compensation test have been applied. Generally, test methods can be divided into contact and noncontact measurements [11]. Con-

* Corresponding authors at: Changchun Institute of Optics, Fine Mechanics and Physics, Chinese Academy of Sciences, Changchun, Jilin 130033, China.
E-mail addresses: hhx@ciomp.ac.cn (H. Hu), xuedl@ciomp.ac.cn (D. Xue).

https://doi.org/10.1016/j.optlaseng.2022.107350
Received 10 March 2022; Received in revised form 29 September 2022; Accepted 21 October 2022
Available online 29 October 2022

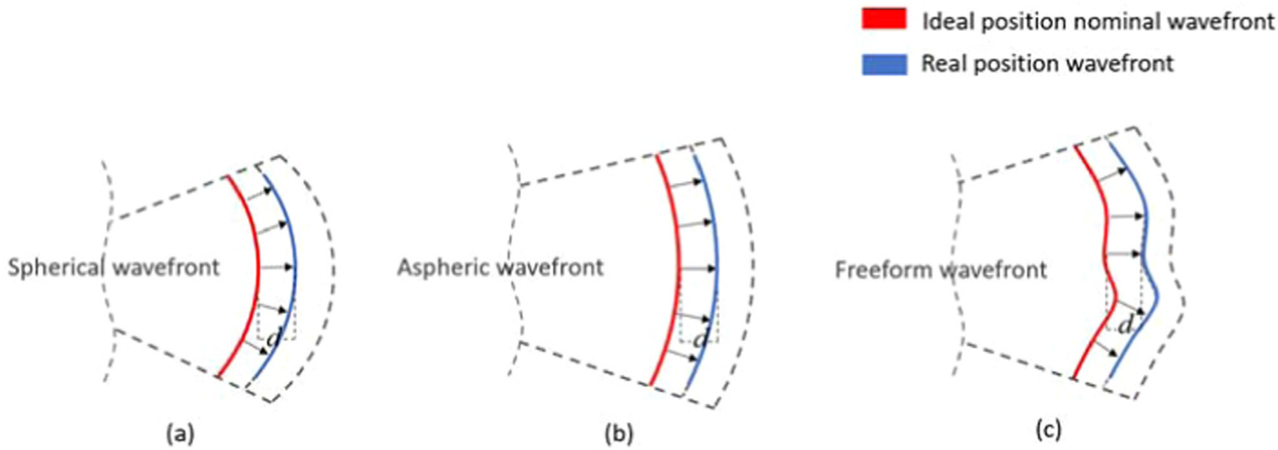

Fig. 1. Sketches of wavefront optical spacing. (a) Spherical surface. (b) Aspheric surface. (c) Freeform surface.

tact measurements mainly include the laser tracker, spherometer, and coordinate measurement machine (CMM) method [12–15]. However, contact measurements pose the risk of scratching the surface [16]. Non-contact measurements have been widely used in many forms to measure the radius of curvature, vertex radius of curvature and conic constant [17,18]. Baiocch and Burge presented a method in which the first two orders of the diffractive wavefront of the hologram were directly projected onto the test board through the projection lens to measure the relative curvature radius error of the segmented mirrors. The measurement accuracy is 30 μm [19]. Yi et al. proposed a compensatory method that employed a separated double lens as a compensator to measure the radius of curvature with a relative error lower than 4.2×10^{-4}. This method requires a long displacement platform [20]. Yang et al. measured the radius of curvature of a sphere based on the wavefront difference method using a pinhole point diffraction interferometer, and the relative measurement precision was of the order of 10^{-4} [21]. Hao et al. proposed partial compensation interferometry measurement system based on the theory of slope asphericity and the best compensation distance to obtain the vertex radius of curvature and conic constant errors. The relative measurement accuracy could be better than 0.02% for the vertex radius of curvature error and 2% for the conic constant error [22]. Pi presented an interferometric method which compares the test surface with a spherical reference wavefront to determine the parent radius of curvature and conic constant of conic surfaces. This method requires moving mirror and measuring distance in addition to interferometric measurement [23]. Although some methods can measure the WOS under the condition of an interferometric compensating test, there are some weaknesses, such as incapability to obtain the absolute error value of the curvature radius, complex installation or algorithm, required long displacement platforms and inapplicability to freeform surface measurements [24,25]. In this study, a method to measure the WOS of freeform surfaces utilizing the principle of computer-generated hologram (CGH) compensation [26–30] and cat-eye interferometry [31] is proposed. An extra cat-eye zone is designed using a traditional CGH compensator. The surface figure and WOS of the freeform mirror can be tested simultaneously with absolute evaluation by employing this method. The experimental device is simple and easy to operate.

The remainder of the paper is organized as follows. In Section 2, the concept of WOS is proposed, and the coupling relationship between the surface error and spacing d is deduced. The cat-eye CGH interferometric method to test the WOS is presented, and the reduction calculations of the spacing d are provided. Simulations and error budgets were also performed. In Section 3, the repeatability experiment and methodology verification of the proposed method are presented. A discussion of the experimental results and conclusions are presented in Sections 4 and 5, respectively.

2. Theory

In the interferometric compensating test, a finely designed compensator (null lens or CGH) was employed to modulate the wavefront to the nominal wavefront matched with the nominal surface at the ideal design position. Owing to the existence of the WOS on the surface, the real testing wavefront differs from the nominal wavefront, resulting in a surface testing error.

By defining the nominal surface as a freeform wavefront in space, this nominal freeform wavefront can be expressed as W_0 (x, y), which is characterised by $W_0(0,0)=0$. The nominal freeform wavefront can be written as:

$$W_0(x,y) = \frac{(x^2+y^2)/R}{1+\sqrt{\left[1-(\kappa+1)(x^2+y^2)/R^2\right]}} + \sum_{i=1}^{n} A_i Z_i(x,y), W_0(0,0)=0 \tag{1}$$

Here, R is the vertex radius of curvature, κ is the conic constant, and Z_i (x, y) and A_i are the Zernike polynomial and coefficient, respectively. Owing to the spacing d, the transformation form of the nominal wavefront is expressed as:

$$p_0\left(x, y, W_0(x,y)\right) \Rightarrow p\left(x+\alpha\cdot d, y+\beta\cdot d, W_0(x,y)+\gamma\cdot d\right) \tag{2}$$

Here, α, β, and γ represent the coordinate components of the normal vector of the nominal freeform wavefront in the x, y, and z directions, respectively. The nominal freeform wavefront's corresponding normal vector can be expressed as:

$$\hat{\mathbf{n}} = \mathbf{n}/|\mathbf{n}| = (\alpha,\beta,\gamma) = \frac{1}{\sqrt{\left(\frac{\partial W_0}{\partial x}\right)^2+\left(\frac{\partial W_0}{\partial y}\right)^2+1}}\left(-\frac{\partial W_0}{\partial x}, -\frac{\partial W_0}{\partial y}, 1\right) \tag{3}$$

The existence of spacing d causes a surface testing error. The expression between the surface testing error δW and spacing d is as follows:

$$\delta W = \frac{d}{1-\gamma} = d\cdot\frac{\left(\frac{\partial W_0}{\partial x}\right)^2+\left(\frac{\partial W_0}{\partial y}\right)^2+1+\sqrt{\left(\frac{\partial W_0}{\partial x}\right)^2+\left(\frac{\partial W_0}{\partial y}\right)^2+1}}{\left(\frac{\partial W_0}{\partial x}\right)^2+\left(\frac{\partial W_0}{\partial y}\right)^2} \tag{4}$$

The aberrations caused by spacing d can be obtained from the above equation. Considering the aspheric surface as an example, the relationship between the spacing-introduced geometric parameter R' and spacing d on the vertex radius of curvature can be written as:

$$R' = R - d \tag{5}$$

The positive spacing d is shown in Fig. 1, and the radius of curvature of the concave surfaces from left to right is negative.

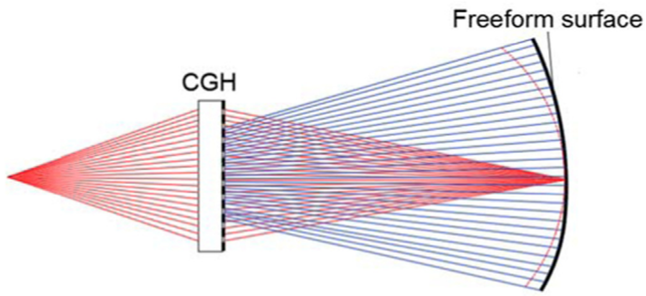

Fig. 2. Cat-eye optical layout diagram.

In the case of d≪*R*, derived from the geometric relationship, the spacing-introduced conic constant *κ'* can be expressed as:

$$\kappa' = \kappa + (d/R) \cdot \kappa \tag{6}$$

The WOS impacts the optical element and not just the radius of curvature. For example, the WOS results in curvature radius and conic constant changes in the aspheric surface, which affect the tolerance distribution of the optical design. For freeform surfaces, the impact on the wavefront is complex. Therefore, under the condition of interferometric compensation, it is necessary to develop an appropriate method for testing the spacing *d* of the freeform surfaces.

2.1. Refine description of cat-eye CGH

The cat-eye interferometry test method has been extensively adopted for the curvature radius measurements of spherical surfaces. When the measured surface is at the cat-eye position, the spherical wavefront emitted by the interferometer is reflected by the measured surface and symmetrically returns to the interferometer to form the cat-eye position interferometry. The wavefront of traditional cat-eye interferometry is produced by a standard spherical lens, and a long rail is required to measure surfaces with large curvature radius [31,32].

In the CGH interferometric compensating test, our designed CGH compensator modulates the original divergent spherical wavefront to a convergent spherical wavefront, and the convergence point is at the position of the nominal surface. The point on the freeform surface, whose normal direction is perpendicular to the CGH, is regarded as the cat-eye position. Through the optical layout, the surface figure is measured by a nominal freeform wavefront (blue divergent beam), while the WOS is measured by a convergent wavefront (red convergent beam), both generated by the CGH simultaneously, as shown in Fig. 2.

According to Eq. (7) [33]:

$$\Delta w(x, y) = -d \cdot \frac{1}{8F^2} \tag{7}$$

Here, *d* is the distance error at the cat-eye position and Δw represents the wavefront change due to the induced distance error, which is expressed as the peak-to-valley (PV) of the power. *F=f/D*, where *f* is the focal length and *D* is the entrance pupil diameter. The spacing *d* can be obtained from positive or negative power values.As shown in Fig. 3, three zones were designed on the CGH to accurately test the WOS of the freeform mirror. These are the alignment, cat-eye, and main zones. The alignment zone wavefront is aimed at aligning the interferometer with the CGH. The main zone wavefront can be used to test the freeform surface. Simultaneously, the cat-eye zone wavefront was employed to test the WOS. To roughly align the interferometer and freeform mirror, four fiducial zones projecting four marks around the mirror edge were added around the CGH main zone.

Because of the coupling relationship between the surface error and the WOS, their measurements should be performed on the same benchmark, and high-precision spacing *d* testing is based on high-precision surface figure testing. In the testing, the alignment zone and main zone aberrations are appropriately adjusted to the minimum to align the interferometer, CGH compensator, and freeform mirror. In this case, the freeform surface can be tested through the main zone wavefront, and the WOS through the cat-eye zone wavefront.

According to the principle of geometric optical imaging,

$$\frac{1}{l} + \frac{1}{l'} = \frac{1}{f'} \tag{8}$$

where *l* is the distance from the focus of the interferometer to the CGH, *l'* is the distance from the CGH to the mirror, and *f '* is the equivalent focal length of the CGH. After differentiating both sides of Eq. (8), the following is obtained:

$$\xi = \left(1 - \frac{l'^2}{l^2}\right)\varepsilon_z \tag{9}$$

Here, ε_z is the position error of the CGH and ξ denotes the cat-eye testing error caused by the CGH position error.

The CGH substrate can be equivalently considered as a plane-parallel glass plate, and a slight longitudinal displacement is produced in the optical layout. The displacement *m* can be written as:

$$m = \frac{n-1}{n}t \tag{10}$$

Here, *n* is the substrate refractive index and *t* denotes the thickness of the substrate. Because the CGH scribing surface is on the rear surface [34], the substrate thickness of the CGH must be added to the object-side distance. By substituting Eq. (10) into Eq. (9), we obtain,

$$\xi = \left(1 - \frac{l'^2}{(l+t-m)^2}\right)\varepsilon_z \tag{11}$$

It is necessary to consider the thickness of the CGH substrate, as well as the slight longitudinal displacement generated by the substrate. Eq. (11) yields the spacing *d* error of the mirror caused by the CGH position error.

2.2. Synthesis of calculation formula

According to Eqs. (7) and (11), in the WOS testing, measurement error d_1 caused by the CGH alignment error, measurement error d_2 due to the main zone power (PV) caused by mirror position error, and the measured spacing d_3 through the cat-eye zone can be calculated as follows:

$$\begin{cases} d_1 = \left(1 - \dfrac{l'^2}{\left(l+t-\frac{(n-1)}{n}t\right)^2}\right)\dfrac{4l^2}{D_C^2}\sigma_1 \\ d_2 = \dfrac{4R_0^2}{D_M^2}\sigma_0 \\ d_3 = \dfrac{4l'^2}{D_E^2}\sigma_2 \end{cases} \tag{12}$$

Here, σ_1 denotes the power (PV) of the CGH alignment zone, D_C is the calibre of the CGH alignment zone, D_M is the mirror diameter, R_0 is the distance from the focal point of the interferometer to the mirror, σ_0 is the power (PV) of the main zone, D_E denotes the calibre of the CGH cat-eye zone, and σ_2 represents the power (PV) of the cat-eye zone, as shown in Fig. 4. All the labeled parameters in this figure are positive, and they follow the rule that the beam travels positively from left to right.

According to Eq. (12), the position errors of the CGH and mirror can be compensated, and the spacing *d* with high precision can be derived as

$$d = -d_1 - d_2 + d_3 \tag{13}$$

The diameter of the concave freeform mirror to be analysed was 320 mm. The nominal radius of curvature, R, was −2139.854 mm. The freeform surface of the mirror was represented by standard Zernike polynomials, as listed in Table 1.

The contribution of the power values for each zone to the optical layout was analyzed quantitatively, and the results are presented in Table 2

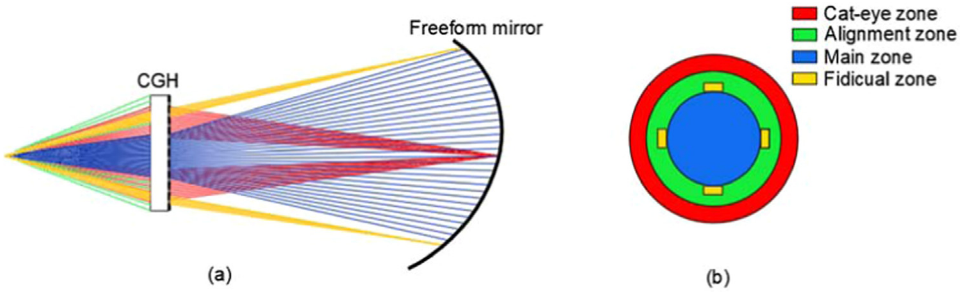

Fig. 3. Optical layout of the freeform surface test with cat-eye CGH. (a) Optical layout diagram. (b) CGH layout diagram.

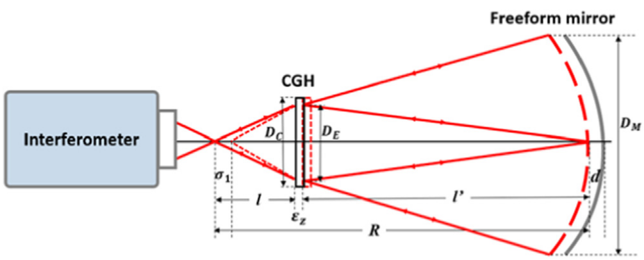

Fig. 4. Schematic of the geometric model for the cat-eye method.

Table 1
Zernike coefficients of the freeform surface (in mm).

Term	Value	Term	Value
a_1	1.680×10^{-2}	a_{14}	1.083×10^{-5}
a_3	-2.150×10^{-2}	a_{17}	3.041×10^{-6}
a_4	1.038×10^{-2}	a_{19}	-8.082×10^{-7}
a_6	-1.148×10^{-1}	a_{21}	-1.050×10^{-7}
a_7	1.631×10^{-2}	a_{22}	4.973×10^{-7}
a_9	1.110×10^{-3}	a_{24}	3.347×10^{-8}
a_{11}	5.300×10^{-4}	a_{26}	-5.594×10^{-9}
a_{12}	1.135×10^{-4}	a_{28}	-1.005×10^{-9}

Table 2
Contribution rate of each zone to the optical layout.

	Power aberration	Effect on the optical layout (μm)	Contribution rate	
			RSS	Monte Carlo
Alignment zone	0.01λ	0.3	0.6%	0.6%
Cat-eye zone	0.01λ	3.7	92.6%	92.9%
Main zone	0.01λ	1.0	6.8%	6.5%

Table 3
Contribution rate of each zone to the spacing d test.

	Power aberration	Effect on the wavefront optical spacing d (μm)	Contribution rate	
			RSS	Monte Carlo
Alignment zone	0.01λ	3.3	42.6%	42.1%
Cat-eye zone	0.01λ	3.7	53.5%	54.0%
Main zone	0.01λ	1.0	3.9%	3.9%

(λ = 632.8 nm, hereinafter inclusive). Table 3 shows the contribution of the power values for each zone to the spacing d test.

According to the performed analysis, the contribution to the spacing d test results is the greatest in the cat-eye zone, followed by the alignment zone, and least in the main zone. As an adjustment value, the CGH position alignment error has a trivial influence on the optical layout, but significantly impacts the spacing d. Therefore, strict adjustment for the alignment zone is needed to attain a high testing accuracy. Furthermore, according to the analysis and Eq. (12), the effect of the alignment zone error on the spacing d is mainly attributed to the ratio of image distance/object distance; therefore, the test sensitivity of the model can be enhanced by altering the ratio of the image to object distances.

ZEMAX® was used to simulate the optical layout to verify the accuracy of the cat-eye CGH method. The same power values were input to both ZEMAX® and the formula, and the results were plotted. The predicted results for the WOS based on calculations and simulations are shown in Fig. 5.

Based on the results in Fig. 5, the simulation and calculation results are consistent when the position error of the CGH does not exist. When the CGH has a position error, there is a deviation in the simulations and calculations. The deviation increased with an increase in the CGH position error. For a CGH position error of 1/10 of the spacing, the estimated error percentage in the calculation and simulation was 2.2%.

The paraxial approximation condition was exploited in the calculation compensation formula for the CGH position error, denoting a deviation between the simulation and calculation results. The position of the CGH can be optically adjusted with a high adjustment accuracy by the alignment zone, resulting in an adjustment accuracy better than 0.5 μm. The adjustment accuracy of the CGH meets the experimental requirements, and the deviation between the simulation and calculation can be ignored.

2.3. Accuracy analysis

Appropriate tolerances were determined by perturbation analysis of each optical layout. There are two major types of errors in the optical layout: systematic and random. Systematic errors mainly include residual design error, CGH fabrication error, and CGH substrate thickness error. The random errors mainly include repeatability errors of the power acquisition in the three zones and temperature errors. All of these errors degrade the accuracy away from the nominal value. Considering the freeform mirror in Section 2.2 for an instance, an accuracy analysis was conducted, as shown in Table 4.

The residual error of the cat-eye path design was 0.006λ power aberration (PV), which has an effect of 2.2 μm on the spacing d test. Based on previous experience, the fabrication error of CGH substrates for power aberration can be controlled to 0.015λ (PV) [35,36]. The refractive index inhomogeneity of the substrate is approximately 2×10^{-6}, which generates a 0.003λ error for the transmitted wavefront through the CGH [35,37], and then has an effect of 1.0 μm on the WOS testing. The thickness of the CGH substrate was measured using the CMM with 1 μm testing accuracy. The thickness error of the CGH substrate causes a large WOS testing error of 7.8 μm. In addition, the repeatability error of the three zones of power acquisition affected the testing results. The F numbers of the main and alignment zones are similar, indicating similar effects of the axial vibration and drift on them, estimated at 0.005λ power aberration (PV) from previous testing experiences. The cat-eye zone optical path was relatively stable with an estimated repeatability testing error of 0.002λ power aberration (PV). Note that the temperature in-

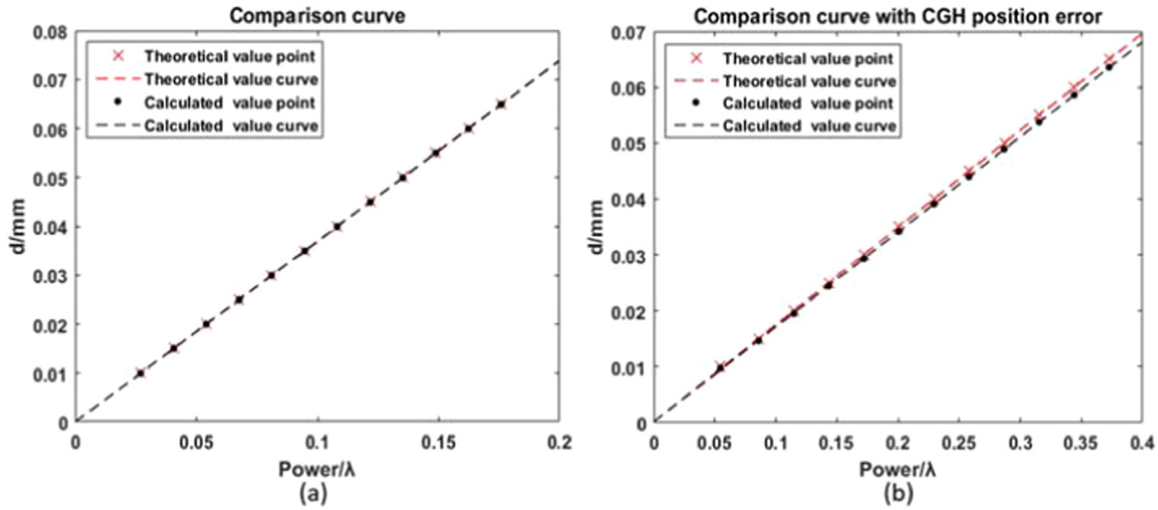

Fig. 5. (a) Spacing *d* comparison curve of calculation and simulation. (b) Comparison curve between calculation and simulation of spacing *d* with CGH position error.

Table 4
Spacing *d* test errors from each error source.

Error type	Sources	Errors (PV)	Impact on the WOS testing
Systematic error	Residual CGH design	0.006λ	2.2 μm
	Fabrication error of CGH	0.015λ [35,36]	1.3 μm
	Refractive index inhomogeneity	2×10^{-6} [35,37]	1.0 μm
	Thickness error of CGH substrate	1.0 μm	7.8 μm
Random error	Repeatability error of power acquisition in alignment zone	0.005λ	1.6 μm
	Repeatability error of power acquisition in main zone	0.005λ	0.5 μm
	Repeatability error of power acquisition in cat-eye zone	0.002λ	0.7 μm
	Temperature error °C	0.1°C	0.4 μm
	Monte Carlo synthesis		8.5 μm

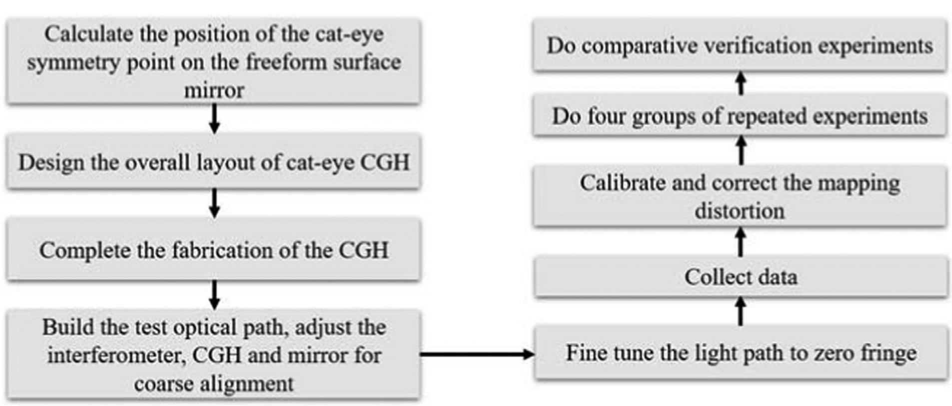

Fig. 6. Flowchart of the test experiment using the cat-eye CGH for freeform surface mirror.

stability affects the laser wavelength, and thus the power measurement, which affects the spacing *d* testing, is approximately 0.4 μm. These errors are commonly independent of each other. The influence of the total errors on the spacing *d* test results is estimated to be 8.5 μm by Monte Carlo synthesis.

3. Experiment verification

3.1. Setup

Experiments are conducted to demonstrate the performance of the proposed method. A flowchart of the experiment is shown in Fig. 6.

We considered the freeform mirror in Section 2.2 as the sample for the experiment. For the freeform mirror, the point whose normal line on the freeform mirror is parallel to the optic axis is regarded as the symmetrical point of the cat-eye optical layout. By calculation, the coordinates of the point on the mirror are (0, −2.791 mm, -1.736×10^{-3} mm). The distance from the interferometer focus to the front is 470 mm and the distance from the CGH to the freeform mirror was 1690.626 mm. The CGH substrate was Corning® 7980 fused silica, and its thickness was 14.823 mm.

As the power aberration is rotationally symmetrical, the radial distribution of the power value in the CGH layout is more important for the test. To obtain a more accurate power value and validate the correctness of the method, a large radial distribution was designed on the CGH. Considering the relationship among the cat-eye zone, main zone, and alignment zone to fully use the CGH, the designed CGH layout is shown in Fig. 7. Two pairs of 16 mm × 45 mm cat-eye zones were de-

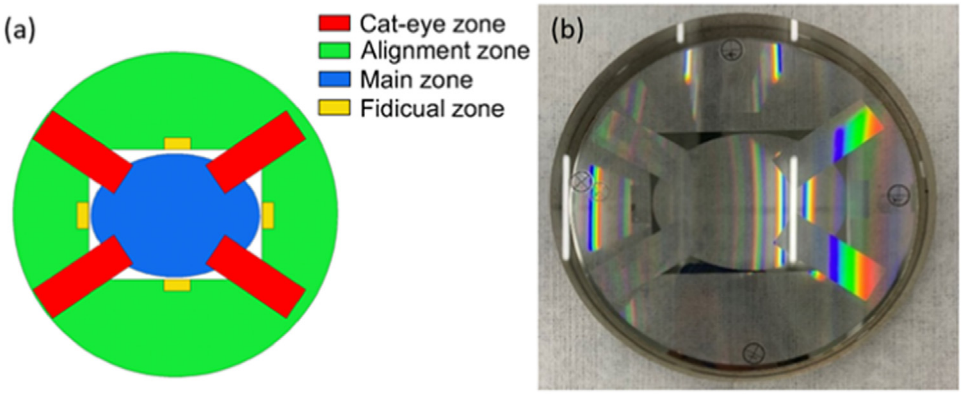

Fig. 7. (a) Layout design of the cat-eye CGH. (b) CGH used in the experimental measurement.

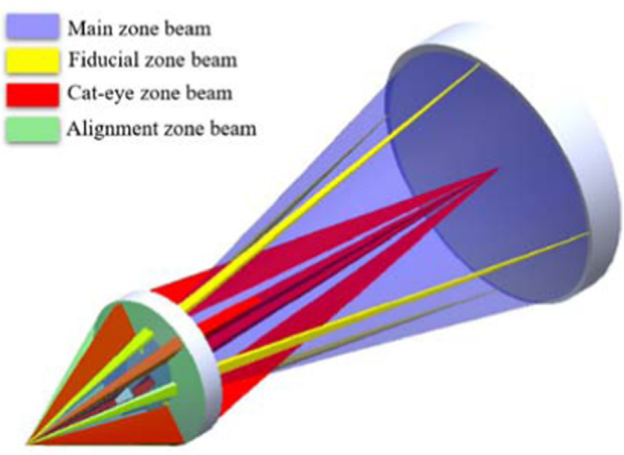

Fig. 8. Designed testing optical layout for the freeform mirror.

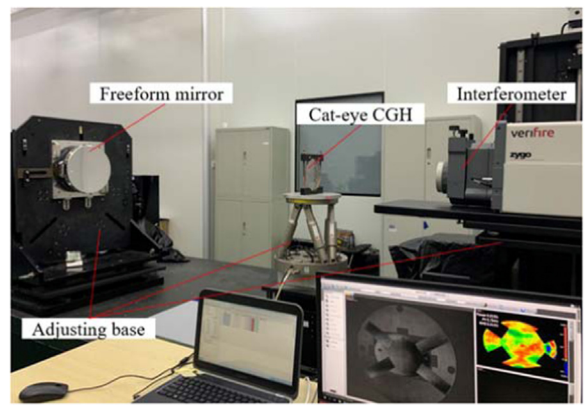

Fig. 9. Experiment setup of the freeform mirror using cat-eye CGH method.

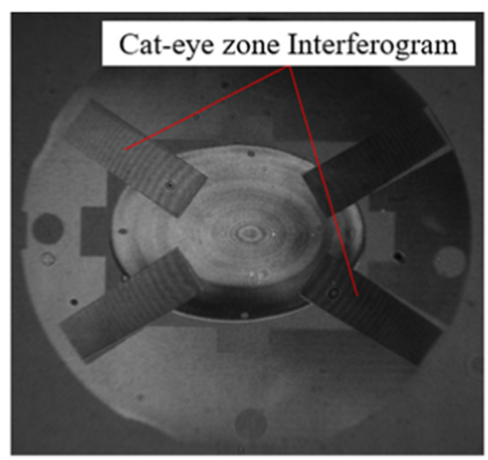

Fig. 10. Interferogram of the testing optical layout.

signed, considering the calculated point mentioned above as the center of symmetry on the CGH of ⌀140 mm. Fig. 7(a) shows the CGH design structure diagram of the freeform mirror, and Fig. 7(b) shows the fabricated CGH used in the measurement, which is an amplitude CGH using the 1st order diffraction wavefront.

A diagram of the optical testing layout is presented in Fig. 8. The yellow beam represents the fiducial wavefront for a coarse alignment between the interferometer and mirror. The green beam represents the wavefront reflected by the CGH. The blue beam represents the main-zone test wavefront. The red beam is for the cat-eye zone wavefront and is reflected at the calculated cat-eye-positioned point of the freeform surface mirror. The optical layout of the experiment is shown in Fig. 9.

During the verification experiment, the room temperature was controlled within 21.7 ± 0.1 °C, considering the effects of the thermal field on optical curvature [38]. The interferometer, CGH, and mirror were roughly adjusted and aligned. Fine adjustments and alignment were performed according to the interferogram pattern. The position of the CGH was fine-adjusted using the interferogram in the alignment zone such that the positional accuracy was better than 0.5 μm.

3.2. Freeform test result

When we adjusted the interferogram to zero fringes in the main and alignment zones, the interferogram in the cat-eye zone was performed as a power aberration, as shown in Fig. 10. In this condition, we completed the testing and data collection.

The mapping distortion of the sample data was corrected using SLAM software (developed by CIOMP). Subsequently, precise interferogram data were obtained, as shown in Fig. 11.

After disrupting the optical layout, the entire process was repeated four times to collect four sets of data, and each set of data was averaged over the ten samples. The power values of the three zones of the four groups of experiments are listed in Table 5.

The collected data were calculated using Eqs. (12) and (13), and the WOS data for the freeform mirror were obtained, as shown in Table 6.

The WOS average value and repeatability [39] of the experiments were −19.9 ± 4.5 μm (P = 95%). Because the radius of curvature is −2139.854 mm, the relative accuracy of the radius of curvature is 2.1 ppm.

In the experiment, the contribution rate of each zone to the WOS repeatability error was systematically analyzed, as shown in Table 7. In

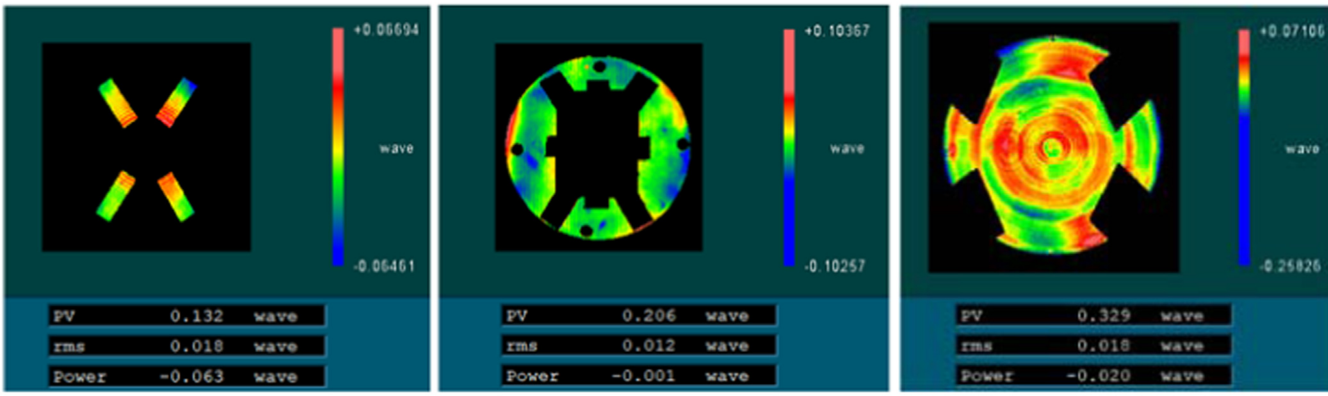

Fig. 11. Group data of three zones. (a) Cat-eye zone result. (b) Alignment zone result.

Table 5
Power (PV) values of three zones.

Group	The power of cat-eye zone	The power of alignment zone	The power of main zone
1	−0.063λ	−0.001λ	−0.020λ
2	−0.057λ	0.007λ	−0.014λ
3	−0.057λ	−0.005λ	−0.035λ
4	−0.056λ	0.010λ	−0.038λ
Standard deviation	0.003λ	0.006λ	0.010λ

Table 6
Data of WOS testing by cat-eye CGH method.

Group	Temperature	Data of WOS d testing by cat-eye CGH (μm)	Repeatability (2σ)
1	21.7 °C	−21.1	4.4 μm
2	21.7 °C	−16.1	
3	21.7 °C	−20.3	
4	21.7 °C	−21.9	

the experimental process, the alignment zone was the major contributor to repeatability error.

The second set of experiments was conducted. The freeform mirror was shifted along the optical axis, and in this case to test the WOS. The test results for the WOS using the cat-eye CGH are listed in Table 8.

The experimentally result with the longitudinal misalignment is −20.2 ± 6.4 μm(P = 95%). The experimental results further proved that the WOS calculation in Eq. (13) of the cat-eye CGH method was correct. However, the tilt error with mirror shifting results in an extra error in the WOS testing.

3.3. Methodology verification

The absolute accuracy of the cat-eye CGH method was also cross-checked with a methodological comparative verification experiment, whose testing accuracy was approximately ±9 μm (±2σ, 16 μm+0.8 μm/m) [40,41]. Four sets of experiments were conducted, and the results are provided in Table 9.

The combined standard uncertainty of the comparative experiment was 10.8 μm. The average value and repeatability [39] of the comparative tests were −9.7 ± 10.8 μm (P = 95%). The agreement between the cat-eye CGH experiment and comparative experiment was 10.2 ± 4.3 μm (P = 95%), so the metrology accuracy of the cat-eye method was 10.2 ± 4.3 μm (P = 95%) [42]. The aforementioned tests confirmed the correctness of the cat-eye CGH method for measuring WOS.

4. Discussion

Using the measured spacing d (−0.019 mm), the testing error on the freeform surface can be obtained by numerical simulations using Eq. (4), as shown in Fig. 12(a), which includes the error in the curvature radius. However, the existence of d introduces other testing errors in addition to the curvature radius error, as shown in Fig. 12(b). The extra testing error was 0.003λ root mean square (RMS), except for the curvature radius error. Because the value of the spacing d is small, the extra testing error is not noticeable.

Assuming that the spacing d is as large as −0.44 mm, the testing error on the freeform surface could be obtained by standard Zernike polynomial fitting, as shown in Table 10.

When the spacing d was −0.019 mm, the power term mainly affected the surface, with astigmatism and coma having a slight influence on the surface. However, when WOS d is increased to −0.44 mm, the influence of astigmatism and coma on the surface is greater than λ/100 RMS, independently, which is not negligible. As a general rule, the larger the WOS d introduced, the more aberrations that affect the surface testing.

When the spacing d value is as large as −0.44 mm, the testing error on the surface caused by the spacing d is shown in Fig. 13(a). In addition to the curvature radius error, the extra testing error was 0.068λ RMS, as shown in Fig. 13(b), including astigmatism mainly. During the optical system adjustment, astigmatism can be adjusted by the decentre in the geometric parameters within the tolerance range. The aberration introduced by the 0.133 mm decentre is shown in Fig. 13(c). The decentre introduces an extra 11.2 μm spacing d, along with astigmatism. The astigmatism generated by a decentre of 0.133 mm is shown in Fig. 13(d). Assuming that the decentre can be conditioned to adjust

Table 7
Each zone contribution rate to the repeatability error.

	Power deviation	Effect on the optical layout (μm)	Effect on spacing d (μm)	Contribution rate
Cat-eye zone	0.003λ	1.1	1.1	20.6%
Alignment zone	0.006λ	0.2	2.0	64.0%
Main zone	0.010λ	1.0	1.0	15.4%

Table 8
Power (PV) values of each zone and calculated results.

The power ofmain zone	The power ofalignment zone	The power ofcat-eye zone	Spacing d (μm)	Repeatability (2σ)
0.214λ	0.014λ	0.009λ	−21.7	6.4 μm
0.090λ	0.019λ	-0.011λ	−19.2	
-0.12λ	0.025λ	-0.075λ	−24.4	
-0.19λ	0.018λ	-0.076λ	−15.7	

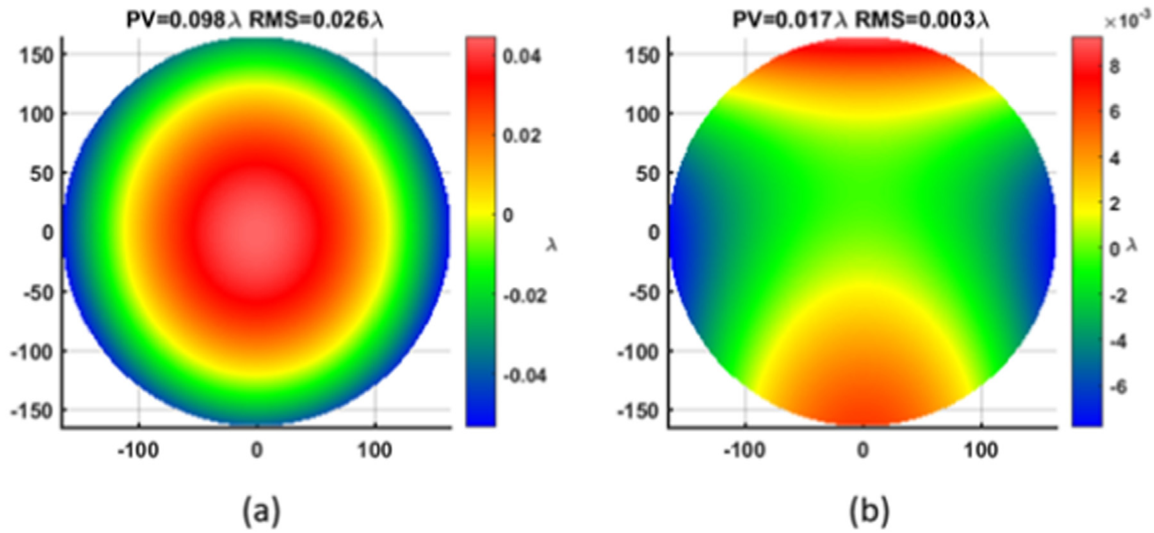

Fig. 12. (a) Aberration on surface caused by testing spacing d. (b) Extra aberration eliminated radius of curvature error caused by testing spacing d.

Table 9
Test results of comparative experiment.

Group	Comparative experiment d (μm)	Repeatability (2σ)
1	−8.4	5.9 μm
2	−11.4	
3	−13.4	
4	−5.5	

Table 10
Testing results of Zernike coefficients difference on the freeform surface (in mm).

Term	Value	Term	Value
a_1	-5.9045×10^{-4}	a_{15}	-1.4331×10^{-11}
a_2	-1.2548×10^{-6}	a_{16}	-2.5619×10^{-10}
a_3	1.1887×10^{-5}	a_{17}	-1.3240×10^{-8}
a_4	-3.4055×10^{-4} *	a_{18}	-4.5680×10^{-13}
a_5	2.2717×10^{-8}	a_{19}	-4.3703×10^{-9}
a_6	-4.2368×10^{-5} *	a_{20}	-3.0189×10^{-13}
a_7	8.8088×10^{-6} *	a_{21}	-5.2031×10^{-10}
a_8	1.1079×10^{-9}	a_{22}	1.3505×10^{-11}
a_9	1.0130×10^{-6} *	a_{23}	-3.4296×10^{-13}
a_{10}	5.2708×10^{-10}	a_{24}	-4.0550×10^{-10}
a_{11}	1.9817×10^{-7} *	a_{25}	-9.1391×10^{-14}
a_{12}	1.9180×10^{-7} *	a_{26}	-9.1241×10^{-11}
a_{13}	-8.9757×10^{-11}	a_{27}	3.8276×10^{-15}
a_{14}	7.2244×10^{-8}	a_{28}	-1.2536×10^{-11}

Note: * The Zernike term indicates that the impact of the term on the surface is greater than $\lambda/1000$ RMS.

the astigmatism, the residual aberration is shown in Fig. 13(e), which cannot be ignored.

When the radius of curvature error and decentre in the geometric parameters are compensated and adjusted, respectively, the influence of spacing d on the freeform surface is $>\lambda/100$ RMS coma and 0.133 mm *y-decentre*.

When the geometric parameters of the freeform surface are compensated and adjusted, the surface error will be reduced to some extent; however, there will be some residual surface errors, which affect the use of the mirror. Therefore, in tolerance balancing, we should consider not only the change in curvature radius but also other errors, which can be obtained by spacing d testing. Furthermore, the analytical form of the WOS test results can be highly beneficial for optimizing the redesign of optical systems.

5. Conclusion

In this study, the concept of the WOS is proposed, and the coupling relation between surface error and WOS is analyzed based on the principle of the interferometric compensating test. We also propose a cat-eye CGH method to simultaneously measure freeform surfaces and the WOS. We designed an interferometry test ray path. Three zones on the cat-eye CGH helped perform an accurate test of the WOS. The contribution of each zone and the accuracy of this method were analyzed. According to the experimental results, the absolute test accuracy of the WOS was 10.2 ± 4.3 μm (P = 95%) (methodological verification), repeatability was 4.5 μm, and relative accuracy was 2.1 ppm.

This method can measure the WOS of optical freeform surfaces under interferometric compensating tests, including the curvature of the sphere radius and the center curvature radius of the aspheric. This method contributes to a high testing accuracy with a simple configuration. The surface testing error caused by the WOS is discussed and explained. This can be effectively employed to guide the tolerance balancing and redesign of optical systems. Future work can focus on improving the applicability of WOS measurement of mirrors with central obstructions by altering the position of the symmetrical return point on the mirror.

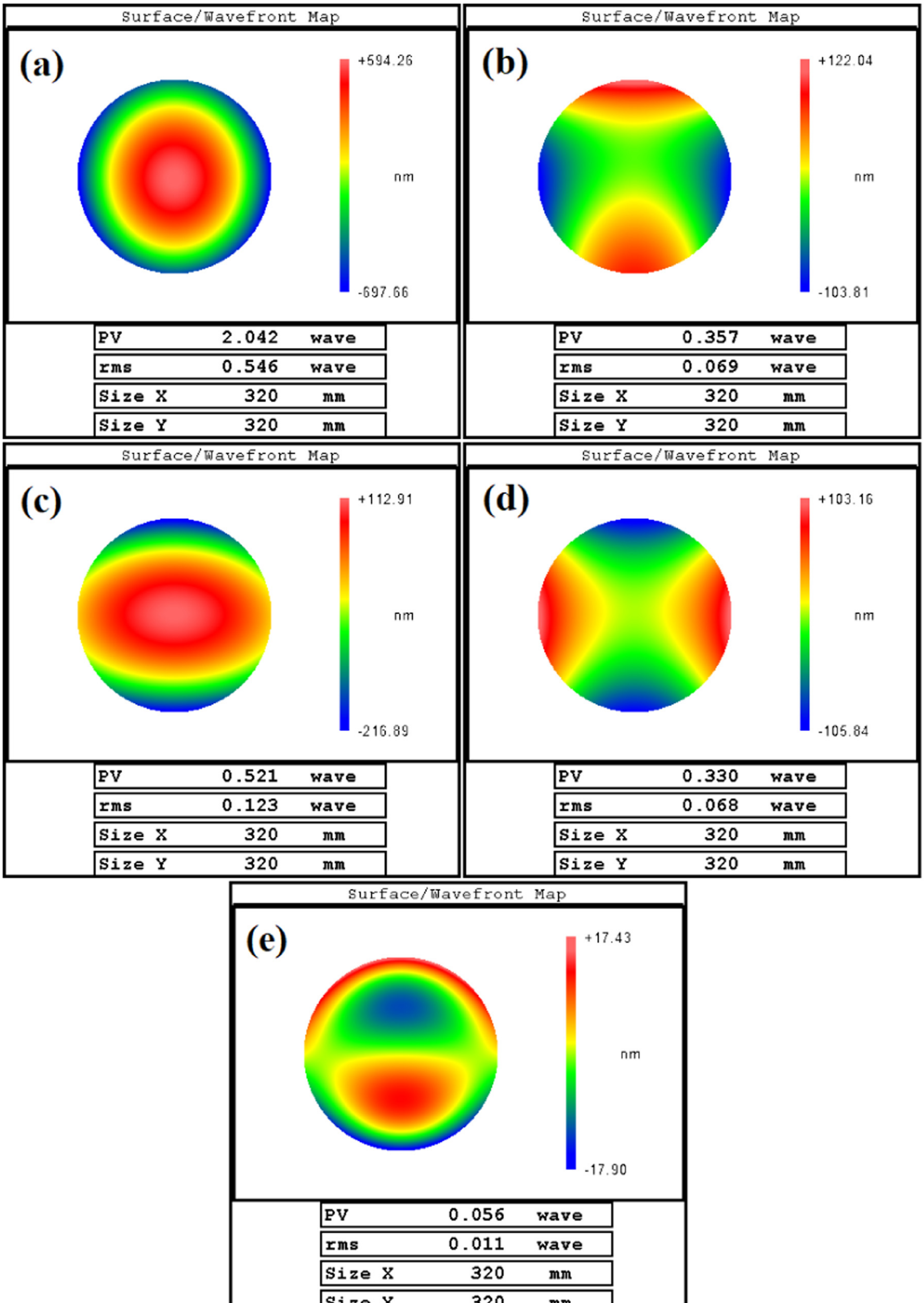

Fig. 13. (a) Aberration on surface when spacing d is −0.44 mm. (b) Extra aberration eliminated radius of curvature error when WOS d is −0.44 mm. (c) Aberration caused by 0.133 mm decenter value. (d) Astigmatism caused by 0.133 mm decenter value. (e) Residual aberration removing geometric parameters.

Funding

This work was supported by Key Research Program of Frontier Science, Chinese Academy of Sciences (QYZDJ-SSW-JSC038), Youth Innovation Promotion Association of the Chinese Academy of Sciences (2019221) and Bureau of International Cooperation, Chinese Academy of Sciences (181722KYSB20180015). This work was partially supported by the National Natural Science Foundation of China (61805243, 62075218, 12003034, 62127901).

Disclosures

H. Hu, X. Zhang, Q. Cheng, D. Xue, and X. Zhang are inventors on a patent application (CN202110354887.4) relating to the freeform mirror WOS measurement described in this paper.

Declaration of Competing Interest

None.

CRediT authorship contribution statement

Xin Zhang: Conceptualization, Investigation, Formal analysis, Data curation, Writing – original draft. **Haixiang Hu:** Supervision, Funding acquisition, Methodology, Writing – review & editing. **Donglin Xue:** Supervision, Funding acquisition, Visualization, Resources, Writing – review & editing. **Qiang Cheng:** Formal analysis, Visualization. **Xi Yang:** Investigation, Software. **Wa Tang:** Resources, Project administration. **Guanbo Qiao:** Writing – review & editing, Data curation. **Xuejun Zhang:** Resources, Funding acquisition.

Data Availability

Data will be made available on request.

References

[1] Ye J, Chen L, Li X, Yuan Q, Gao Z. Review of optical freeform surface representation technique and its application. Opt Eng 2017;56:1. doi:10.1117/1.OE.56.11.110901.
[2] Winsor RS, Mac Kenty JW, Stiavelli M, et al. Optical design for an Infrared Multi-Object Spectrometer (IRMOS). Proc SPIE 2000;4092:4092. doi:10.1117/12.402425.
[3] Yunfeng N, Rubén M, Pablo B, et al. Optical design of an ultrashort throw ratio projector with two freeform mirrors. Proc SPIE 2016;9947:99470C. doi:10.1117/12.2236613.
[4] Yang G, Dewen C, Chen X, et al. Design of an ultrashort throw catadioptric projection lens with a freeform mirror. Proc SPIE 2016;10154:101540S. doi:10.1117/12.2246499.
[5] Cheng D, Wang Y, Hua H, Talha MM. Design of an optical see-through head-mounted display with a low f-number and large field of view using a freeform prism. Appl Opt 2009;48:2655–68. doi:10.1364/AO.48.002655.
[6] Schöck M, Do T, Ellerbroek BL, et al. Thirty meter telescope astrometry error budget. Int Soc Opt Photonics 2014. doi:10.1117/12.2057089.
[7] Chaney DM, Saif BN, Greenfield PE, et al. JWST center of curvature test method and results. Astron Opt Des Manuf Test Space Ground Syst 2017. doi:10.1117/12.2273974.
[8] ISO - ISO 10110-1:2019 - Optics and photonics — Preparation of drawings for optical elements and systems — Part 1: General https://www.iso.org/standard/57574.html.
[9] Burge JH. Applications of computer-generated holograms for interferometric measurement of large aspheric optics. Proc SPIE Int Soc Opt Eng 1995;2576:258–69. doi:10.1117/12.215609.
[10] Liu J, Thomson MJ, Waddie AJ. Design of diffractive optical elements for high-power laser applications. Opt Eng 2004;43. doi:10.1117/1.1803553.
[11] Murty MVRK, Shukla RP. Measurement of long radius of curvature. Opt Eng 1983;22:231–5. doi:10.1117/12.7973089.
[12] Cooke F. The bar spherometer. Appl Opt 1964;3:87–8. doi:10.1364/AO.3.000087.
[13] Wang X, Zheng L. A method for testing radius of curvature of optical spheric surface. Acta Opt Sin 2011;08:166–70. doi:10.3788/AOS201131.0812010.
[14] Zhao C, Zehnder R, Burge J. Measuring the radius of curvature of a spherical mirror with an interferometer and a laser tracker. Opt Eng 2005;44:090506. doi:10.1117/1.2047594.
[15] Chen X, Li R. Research on geometric parameter measurement method using laser tracker in null lens asphere testing. Chin J Lasers 2015;42(5):0508007. 10.3788/CJL201542.0508007.
[16] Jiang W, Cho MK, Wu F, et al. A new method on measuring radius of curvature of a conic aspherical mirror. In: Proceedings of the international symposium on advanced optical manufacturing & testing technologies: Large mirrors & telescopes. International Society for Optics and Photonics; 2014.
[17] Hao Q, Li T, Hu Y, Wang S, Ning Y, Tan Y, et al. Vertex radius of curvature error measurement of aspheric surface based on slope asphericity in partial compensation interferometry. Opt Express 2017;25:18107–21. doi:10.1364/OE.25.018107.
[18] Yao H, Hao Q, Li T. Partial compensation interferometry for measurement of surface parameter error of high-order aspheric surfaces. International Conference on Optical Instruments and Technology. Opt Syst Mod Optoelectron Instrum 2017;2018. doi:10.1117/12.2292278.
[19] Baiocchi D, Burge JH. Radius of curvature metrology for segmented mirrors. Proc SPIE Int Soc Opt Eng 2000;4093:58–67. doi:10.1117/12.405241.
[20] Yi H, Zhang R, Hu X, Peng Y, Zhang K, Chen M. A novel compensation method for the measurement of radius of curvature. Opt Laser Technol 2011;43:911–15. doi:10.1016/j.optlastec.2010.09.014.
[21] Yang Z, Gao Z, Yuan Q, Ye J, Li M. Radius of curvature measurement based on wavefront difference method by the point diffraction interferometer. Opt Lasers Eng 2014;56:35–40. doi:10.1016/j.optlaseng.2013.12.008.
[22] Hao Q, Li T, Hu Y, Wang S, Ning Y, Chen Z. Partial compensation interferometry measurement system for parameter errors of conicoid surface. Rev Sci Instrum 2018;89(6):063102. doi:10.1063/1.5027146.
[23] Pi Y, Reardon PJ. Determining parent radius and conic of an off-axis segment interferometrically with a spherical reference wave. Opt Lett 2007;32(9):1063–5 May 1. doi:10.1364/ol.32.001063.
[24] Huang C, Wu Y, Fan B, et al. Solving surface parameters of conic asphere mirror based on computer simulation. In: Proceedings of the 8th international symposium on advanced optical manufacturing & testing technology. International Society for Optics and Photonics; 2016.
[25] Chen S, Xue S, Zhai D, Tie G. Measurement of freeform optical surfaces: trade-off between accuracy and dynamic range. Laser Photonics Rev 2020;14. doi:10.1002/lpor.201900365.
[26] Kim T, Burge JH, Lee Y, Kim S. Null test for a highly paraboloidal mirror. Appl Opt 2004;43:3614–18. doi:10.1364/AO.43.003614.
[27] Song JB, Yun WL, Lee HY, et al. Optical test for the primary mirror of a space telescope using a CGH null lens. Proc SPIE 2006;6034. doi:10.1117/12.668159.
[28] Davies AD, Schmitz TL. Defining the measurand in radius of curvature measurements. Proc SPIE Int Soc Opt Eng 2003;5190:134–45. doi:10.1117/12.504884.
[29] Lee WH. Binary computer-generated holograms. Appl Opt 1979;18:3661–9. doi:10.1364/AO.18.003661.
[30] Lohmann AW, Paris DP. Binary Fraunhofer hologram, generated by computer. Appl Opt 1967;6:1739–48. doi:10.1364/AO.6.001739.
[31] Selberg LA. Radius measurement by interferometry. Proc SPIE Int Soc Opt Eng 1992;31:1961–6. doi:10.1117/12.59905.
[32] Yang Y, Zhang L, Shi T, Liu D, Chong S, Shen Y, et al. Determination of aspheric vertex radius of curvature in non-null interferometry. Appl Opt 2015;54:2838–44. doi:10.1364/AO.54.002838.
[33] Simon F, Khan G, Mantel K, Lindlein N, Schwider J. Quasi-absolute measurement of aspheres with a combined diffractive optical element as reference. Appl Opt 2006;45:8606–12. doi:10.1364/ao.45.008606.
[34] Kim T, Burge JH, Lee Y. Measurement of highly parabolic mirror using computer-generated hologram. Proc SPIE Int Soc Opt Eng 2002;4778:119–26. doi:10.1117/12.473534.
[35] Zhou P, Burge JH. Fabrication error analysis and experimental demonstration for computer-generated holograms. Appl Opt 2007;46:657–63. doi:10.1364/AO.46.000657.
[36] Hao T. The fabrication of high accuracy phase computer generated hologram by physical vapor deposition. Changchun Institute of Optics, Fine Mechanics and Physics; 2017. Chinese Academy of Sciences. doi:10.1364/AO.57.000F31.
[37] Zhang H, Wang X, Xue D, Zhang X. Modified surface testing method for large convex aspheric surfaces based on diffraction optics. Appl Opt 2017;56:9398–405. doi:10.1364/AO.56.009398.
[38] Jie M, Xi H, Fan W. The effects of thermal field on radius of curvature interferometric testing. Opt Rev 2015;22:299–307. doi:10.1007/s10043-015-0071-z.
[39] ISO International vocabulary of basic and general terms in metrology. 2nd ed ISO guide 99:2007. Geneva, Switzerland: International Organization for Standardization; 1993.
[40] Li R, Wang X, Zheng L, Zhang X. Method of measuring the deviation of curvature radius of aspheric vertex with laser tracker. Chinese patent: CN102288132A, 2011–12-21.
[41] Li J, Wu F, Wu S, Kuang L. A method for measuring the radius of curvature of aspheric vertices by laser tracker. Chinese patent: CN102506761 B, 2012-06-20.
[42] Bertsekas DP, Tsitsiklis JN. Introduction to probability. Athena Scientific; 2008.